Supporting Information

Chang et al. 10.1073/pnas.0913302107

SI Text

Materials and Methods. ***Protein expression and purification.*** The biofilm-forming *S. epidermidis* strain ATCC 35984 (RP62A) was obtained from the Food Industry Research and Development Institute in Taiwan. The *TcaR* gene was amplified directly from the *S. epidermidis* RP62A genome by polymerase chain reaction (PCR) with forward 5′-GGAATTC*CATATG*CACCACCAC-CACCACCACATGGTAAGAAGAATAG-AA GATCACATC-3′ and reverse 5′-CCC*AAGCTT*TCA AAGTTTAGAAGTATAA-GATTGTAT-3′ primers. The PCR product encoding *TcaR* with an amino-terminal His_6 tag was digested with *NdeI* and *HindIII* and subsequently cloned into expression vector pET-21 (Novagen). This construct was transferred into *Escherichia coli* of Arctic Express™ (DE3) RIL strain. DNA sequencing was performed to confirm the appropriate orientation. The His_6-tagged wild-type protein was overexpressed in Difco Luria–Bertani (LB) broth containing 50 mg/L ampicillin to an optical density at 600 nm of 0.5–0.6 and then induced with 0.5 mM IPTG. Cells were grown for 2 days at 13 °C. The cells were then harvested by centrifugation at 12000 g for 30 min and disrupted by Constant Cell Disruption System (Constant System Ltd) with lysis buffer containing 20 mM Tris-HCl (pH 8.5), 400 mM NaCl, and 10 mM imidazole. The homogenate was centrifuged at 27,000 g for 30 min and the cell-free extract was loaded onto a Ni^{2+}-NTA column, which had been previously equilibrated with lysis buffer. The column was washed with lysis buffer, and the His_6-tagged TcaR was subsequently eluted by a linear gradient of imidazole from 10 mM to 500 mM. The fractions containing purified TcaR were collected and dialyzed against three 5 liters of buffer (first, 20 mM sodium citrate, 10% glycerol, 300 mM NaCl, pH 4.5; second, 20 mM sodium citrate, 10% glycerol, 200 mM NaCl, pH 4.5; third, 20 mM sodium citrate, 10% glycerol, 100 mM NaCl, pH 4.5), subsequently for 6 h. The purified His_6-tagged TcaR was finally concentrated by 3 kDa cut-off size membrane of Amicon ultra-15 centrifugal filter units (Millipore) for storage at −80 °C. The molecular weight of the purified protein was verified by mass spectrometry, and the purity (>95%) was measured by SDS-PAGE.

SeMet-labeled TcaR was overexpressed in slightly modified SeMet minimal medium containing 100 mg/L ampicillin at 13 °C for 2 days with 0.5 mM IPTG as an inducer (1). The detailed protocol as follows: 200 mL overnight culture of M9 medium (Na_2HPO_4 6 g/L, KH_2PO_4 3 g/L, NaCl 0.5 g/L, NH_4Cl 1 g/L, 2 mM $MgSO_4$, 0.1 mM $CaCl_2$, 0.4% glucose) of a single transformant was used to inoculate 6 liters of fresh M9 medium containing 100 g/L ampicillin at 37 °C until OD 0.6 at 600 nm, and then cooled to 13 °C. A 120 mL filter-sterilized solution containing 60 mg $Fe_2(SO_4)_3$ and 60 mg thiamine and 600 mg DL-SeMet was divided equally among the 6 l medium. One hour later IPTG was added to a final concentration of 0.5 mM for 2 days induction. Purification of the SeMet–TcaR was performed using the same protocol established for native TcaR. The purified protein was concentrated and stored at −80 °C.

Crystallization and data collection. For crystallization, TcaR and SeMet–TcaR solutions were adjusted to 18 mg/mL in 20 mM sodium citrate, 10% glycerol, 100 mM NaCl, pH 4.5 containing 5 mM DTT. The crystals of TcaR and SeMet–TcaR were obtained with 0.1 M Na-Hepes, pH 7.5, approximately 8–14% PEG4000 and approximately 10–13% 2-propanol precipitant solution. High-quality crystals were grown to full size within 2 days at room temperature. For the ligand-bound crystal forms, the crystals of native TcaR were soaked for 1 h in a solution consisting of 75% mother liquor/25% glycerol/1 mM ligand. The X-ray diffraction data for the Se-Met-labeled TcaR were collected at SPring-8 (Hyogo, Japan), beamline BL12B2 and the native TcaR data were collected for improving resolution at the National Synchrotron Radiation Research Center (NSRRC), BL13B1. All diffraction images were recorded using ADSD Q315 CCD detector and the data were processed and scaled by using the program package of HKL2000 (2). The data collection statistics are summarized in Tables S1 and S2.

Electrophoretic mobility shift assays (EMSA). There are three fragments of possible TcaR binding DNA which were purchased from MDBio Inc.. The three DNA fragments are 33-mer DNA oligonucleotides within the *ica* promoter, labeled as DNA1, DNA2, and DNA3 (Table 1). Double-stranded DNA were prepared by annealing complementary oligonucleotides (100 mM each) in 10 mM Tris-HCl, pH 8.0, 20 mM NaCl, heating the reaction to 95 °C for 5 min and allowing it to cool to 25 °C. A 30 μL binding reaction containing 1–4 μM of purified recombinant TcaR and 1 μM of various dsDNA substrates in binding buffer (20 mM Tris-HCl, pH 8.0, 150 mM KCl, 0.1 mM $MgCl_2$, 0.05 mM EDTA, 12.5% Glycerol, 10 mM DTT and 1 mg/mL BSA) was incubated at room temperature with gentle vortex for 15 min. After incubation, 15 μL of the reaction solution was mixed with 3 μL of the sample loading dye and subsequently loaded onto a 6% nondenaturing polyacrylamide gel and electrophoresed in 1/2 Tris/acetate/EDTA (TAE) at 100 V for 30 min and visualized using SYBR Green I nucleic acid gel stain (Invitrogen). In the assay for effects of antibiotics on the interaction of TcaR and DNA, DNA1 probe of 1 μM was preincubated with 2 μM TcaR (dimer) at room temperature for 15 min before mixing with 2 μM antibiotics, followed by the same procedure as in the other assays.

Computer modeling. Because TcaR structure is similar to other MarR family proteins, the structure of the OhrR-DNA complex from PDB 1Z9C was used as a template to construct a model of TcaR–DNA complex. The 29 bp pseudopalindromic DNA sequence of 1Z9C was mutated to the sequence of Consensus 1 (Table S1) that was used in the EMSA experiment (see below). Using the program O, the new base pairs were positioned as close as possible to match those in the template, whereas the sugar phosphate backbone remained unscathed. Molecular dynamics and energy minimization were subsequently carried out using CNS, with atomic positions of both the protein and the DNA tethered to the originals by applying a moderate harmonic restraint.

Quantitive biofilm assay. To assess biofim formation, inoculums of *S. epidermidis* RP62A was prepared in LB as described previously (3), and incubated for 18 h at 37 °C on a shaker at 200 rpm. The inoculums was diluted 1:20 times in tryptic soy broth (TSB) for *S. epidermidis* and 190 μL each was aliquoted per well on a 96-well polystyrene microtiter plate, and 10 μL each of appropriately concentrated antibiotic was added to each well of 96-well plate. The microtiter plate was incubated at 37 °C. After 24 h incubation, the medium was gently removed and the microtiter plate wells were washed three times with PBS (0.1 M, pH 7.4) buffer. The microtiter plate wells were stained with 200 μL of 0.4% crystal violet for 15 min at room temperature. The unbound crystal violet was removed and the wells were washed gently three times with 200 μL of PBS buffer. The wells were air-dried for 15 min

and the crystal violet in each well was solubilized by adding 200 μL of 95% ethanol. The plate was read at 570 nm using microtiter plate reader.

Protein Data Bank accession codes. The atomic coordinates and structure factors for the native TcaR crystal, TcaR-Sal, TcaR-Amp, TcaR-Kan, TcaR-Meth, and TcaR-PnG have been deposited in the wwPDB with accession numbers of 3KP7, 3KP6, 3KP3, 3KP5, 3KP4, and 3KP2, respectively.

Sequence alignment of TcaR. The structure of TcaR was searched against the PDB using the DALI program to identify structural homologs (4). Numerous DNA-binding proteins were identified from this analysis, with the MarR family protein from *Bacillus stearothermophilus* (PDB ID: 2RDP) being the closest structural match with a Z score of 15.6 followed by a Z score of 14.0 for MarR family protein from *Silicibacter pomeroyi* (PDB ID: 3BJ6), a Z score of 14.0 for hypothetical MarR family protein from *Sulfolobus tokodaii* (PDB ID: 2EB7) (5), a Z score of 14.0 for MarR family protein from *Xanthomonas campestris* (PDB ID: 2FA5) (6), and a Z score of 12.5 for the MarR protein from *E. coli* (PDB ID: 1JGS) (7). The Z score is a measure of structural similarity, with increasing value indicating higher level of structural conservation. The three-dimensional structure of TcaR superposed with the MarR family protein structures from *B. stearothermophilus*, *S. pomeroyi*, *S. tokodaii*, *X. campestris*, and *E. coli* with rmsd values of 3.7, 10.6, 3.5, 4.4, and 4.3 Å, respectively, between the structurally equivalent Cα positions. Although these scores reflect the overall structure similarity between TcaR and these proteins, their amino acid sequences do not share obvious similarities (Fig. S1).

TcaR-DNA complex modeling. Superposition of the TcaR dimer with the OhrR–ohrA operator complex revealed a similar overall topology. Moreover, it is interesting to note that the DNA contacting residues of the wHTH domain in the OhrR protein are highly conserved in TcaR. Superposition of the TcaR wHTH domain (α2-α3-α4-βA-W1-βB) onto the OhrR wHTH domain (α2-β1-α3-α4-β2-W1-β3) showed rmsd of 0.864 Å. Therefore, the DNA binding domain of OhrR was used as a reference when we build the model of the wHTH region in TcaR. We used the crystal structure of OhrR–DNA complex (PDB 1Z9C) as a template to construct a model of TcaR–DNA complex. The double strand sequence Consensus1 as derived from the EMSA results below is shown in Fig. S2*B*, and an overview of modeled TcaR–DNA complex is shown in Fig. S2*A*. In this model, two continuous major grooves of the DNA were bound by the helices of the wHTH motif in TcaR. Another DNA-binding element, the wing, is composed of β-strands and loops which interact with the minor groove of the DNA. Interestingly, Asp92 and Arg94 in the OhrR-DNA complex, equivalent to Asp91 and Arg93 in TcaR, also interact with the minor groove of the DNA. We have noticed that these two residues are highly conserved in the MarR family proteins and the BlaI protein. The previous mutation experiments revealed that Arg94 of *E. coli* MarR and Arg91 of *P. aerugunosa* MexR are important for their DNA-binding affinity (7, 8). Therefore, one of the key residues for the DNA-binding ability of TcaR should be Arg93. In addition, another TcaR–DNA model derived from an alternatively predicted DNA sequence was shown in Fig. S2*C*. Taken together, the complex model suggests that TcaR may recognize its operator DNA by using the same repertoire of interactions of OhrR, with slight variations. Further investigation is needed to elucidate the interaction-forming residues in TcaR.

Comparison of the MarR–salicylate complex structures. The TcaR–Sal complex structure revealed that a large portion of the hinge region between the DNA-binding and the dimerization domains form the hydrophobic ligand binding pocket. The detailed interactions of SAL1-8 are shown in Fig. S5*B–I*. In each of these sites, the salicylate ring sits over a hydrophobic side chain in the pocket. There are three MarR family protein–salicylate complex structures available up to now: *E. coli* MarR (7), *M. thermoautotrophicum* MTH313 (9), and *S. tokodaii* ST1710 (10). Comparison of these salicylate complexes with TcaR revealed that the overall topology is similar (Fig. S5*A*). The salicylate ligands in *E. coli* MarR are highly solvent exposed, which may be important in stabilizing crystal contacts. On the other hand, the ligands in MTH313 and ST1710 both locate toward the α5 helix upon binding. However, TcaR is the one with the most numerous salicylate binding sites and those sites are distinct from other MarR family protein structures solved. Three salicylates (SAL2, SAL3, and SAL4) interact with TcaR within the dimerization domain, one (SAL6) is partially solvent exposed close to the DNA-binding domain, and the other four are bound directly at the junction of the DNA binding and the dimerization domains. Consequently, this observation supports our EMSA studies in which a higher molar ratio of salicylate is needed to occupy all the SAL binding pockets to inactivate TcaR effectively compared with other antibiotics tested. Moreover, because the binding sites of salicylate that we observed are numerous and nonspecific, it seems like salicylate is able to interact, perhaps weakly, with many proteins that possess suitable hydrophobic cavities and thereby influence the biological function of those proteins. This might explain the broad physiological effects of aspirin.

Crystal structure of TcaR complexed with ampicillin. Ampicillin (Amp) is similar to PnG in its bactericidal action against susceptible organisms during the stage of active multiplication. It acts through the inhibition of cell wall mucopeptide biosynthesis (11). Amp has a broad spectrum of bactericidal activity against many gram-positive and gram-negative aerobic and anaerobic bacteria, however, as with other penicillin drugs, it is often resisted by Gram-positive *staphylococci*, including *S. epidermidis* (12). Here, we solved the structure of the TcaR–Amp complex to 3.2 Å resolution by molecular replacement and refined to a R_{work}/R_{free} of 24.7%/27.4% (Table S2). Comparison of apo TcaR with the TcaR–Amp complex reveals a large conformational change in the DNA binding domain, especially on chain B (Fig. S4 *A* and *B*). Interestingly, the shrinkage of distance between two DNA-binding domains in the TcaR–Amp complex is more dramatic than those in the PnG and salicylate complexes, with the distance between the N termini of the $\alpha 4/\alpha' 4$ helices from 31.2 Å for the TcaR–DNA model to 22.5 Å for the TcaR–Amp complex (Cα-Cα distance between Lys A65 and Lys B65), and the C termini of the $\alpha 3/\alpha' 3$ helices from 26.0 Å for the TcaR–DNA model to 15.9 Å for the TcaR–Amp complex (Cα-Cα distance between Asn A61 and Asn B61). These steric movements may produce a protein conformational incompatible with DNA binding activity. Surprisingly, both of the two molecules of Amp are located in chain B, an observation that is different from other antibiotics that we have tested in this work. For a detailed description of the interaction profiles, please see Fig. S6 *A* and *B*.

Crystal structure of TcaR complexed with methicillin. Like the function of other beta-lactam antibiotics, methicillin (Meth) works by inhibiting the synthesis of bacterial cell walls. It inhibits cross-linkage between the linear peptidoglycan polymer chains that make up a major component of the cell wall of Gram-positive bacteria such as *S. aureus* that would otherwise be resistant to most penicillins (13). Meth is insensitive to β-lactamase (also known as penicillinase) enzymes secreted by many penicillin-resistant bacteria. The presence of the *ortho*-dimethoxyphenyl group directly attached to the side chain carbonyl group of the penicillin nucleus facilitates the β-lactamase resistance, because those enzymes are relatively intolerant of side chain steric

hindrance. However, strains of Meth- resistant *S. aureus* and Meth-resistant coagulase-negative *staphylococci* have spread worldwide and have become established outside of the hospital environment, particularly among patients in chronic care facilities and in parenteral drug abusers (14, 15). Our gel-mobility analysis confirmed the ability of Meth to interact with TcaR and to inhibit protein–DNA complex formation. To see how Meth binds to TcaR, we determined the TcaR–Meth complex at a solution of 2.84 Å, and refined to a final R_{work} value of 23.6% and an R_{free} value of 25.6% (Table S2). This is the first Meth-protein complex in the Protein Data Bank. The overall conformation of the complex is similar to apo TcaR structure, with an rmsd of 1.35 Å for superposition of 278 Cα atoms (Fig. S4 *A* and *B*). Nevertheless, a major conformational change was observed in the DNA binding wHTH motifs that twist with the respect to each other to produce a sheared orientation with the most contracted distance between the N termini of the $\alpha4/\alpha'4$ helices to 21.1 Å for the TcaR–Meth complex (Cα-Cα distance between Lys A65 and Lys B65), and the C termini of the $\alpha3/\alpha'3$ helices to 15.3 Å for the TcaR–Meth complex (Cα-Cα distance between Asn A61 and Asn B61). It suggests a mode of regulation in which DNA binding is prevented by steric occlusion on the DNA–TcaR interface. This asymmetric structural change caused by two separate Meth binding sites is similar to the conformational change seen in other TcaR–antibiotic complexes. The detailed interactions of Meth1 and Meth2 are shown in Fig. S6 *C* and *D*.

Crystal structure of TcaR complexed with kanamycin. Kanamycin (Kan) is an aminoglycoside antibiotic which works by affecting the 30S ribosomal subunit and causing a frameshift mutation to suppress the translation of RNA. In addition, it is an antiinfective drug used for treatment of infections when penicillin or other less toxic drugs do not work (16). It is known that Gram-positive *staphylococci* including *S. epidermidis* is resistant to Kan by producing a variety of mechanistically different aminocyclitol-modifying enzymes including the aminocyclitol-3′-phosphotransferase (APH[3′]-III) (17). However, The mechanism of how the MarR family proteins regulate the gene encoding APH[3′]-III remains unclear. Here, we solved the TcaR-Kan complex to a resolution of 2.90 Å and refined to a final R_{work}/R_{free} value of 23.3% and 27.6%, respectively (Table S2). In the overall structure of TcaR-Kan complex shown in Fig. 3*E*, we observed two Kan binding sites that are in the relative binding position as seen in the previous discussed antibiotic. The conformational change caused by Kan is similar to other TcaR-antibiotics complexes discussed above, which show dramatic conformational change in the DNA binding domain, especially in chain B (rmsd values of 1.0 on chain B and 0.7 on chain A) (Fig. S4 *A* and *B*). These conformational changes shorten the C- termini of the $\alpha3/\alpha'3$ helices from 26.0 Å for the TcaR–DNA model to 15.8 Å for the TcaR–Kan complex (Cα-Cα distance between Asn AZA61 and Asn B61) and the N termini of the $\alpha4/\alpha'4$ helices from 31.2 Å for the TcaR-DNA model to 22.0 Å for the TcaR–Kan complex (Cα-Cα distance between Lys A65 and Lys B65), forming a winged helix lobe orientation that is incompatible with DNA binding. For more detailed interaction information of Kan1 and Kan2, please refer to Fig. S6 *E* and *F*.

1. Guerrero SA, Hecht HJ, Hofmann B, Biebl H, Singh M (2001) Production of selenomethionine-labeled proteins using simplified culture conditions and generally applicable host/vector systems. *Appl Microbiol Biotechnol* 56(5–6):718–723.
2. Otwinowski Z, Minor W (1997) Processing of X-ray diffraction data collected in oscillation mode. *Method Enzymol* 276:307–326.
3. Wakimoto N, et al. (2004) Quantitative biofilm assay using a microtiter plate to screen for enteroaggregative *Escherichia coli*. *Am J Trop Med Hyg* 71(5):687–690.
4. Holm L, Sander C (1993) Protein structure comparison by alignment of distance matrices. *J Mol Biol* 233(1):123–138.
5. Chin KH, et al. (2006) The crystal structure of XC1739: A putative multiple antibiotic-resistance repressor (MarR) from *Xanthomonas campestris* at 1.8 A resolution. *Proteins* 65(1):239–242.
6. Martin RG, Rosner JL (1995) Binding of purified multiple antibiotic-resistance repressor protein (MarR) to *mar* operator sequences. *Proc Natl Acad Sci USA* 92(12):5456–5460.
7. Alekshun MN, Levy SB, Mealy TR, Seaton BA, Head JF (2001) The crystal structure of MarR, a regulator of multiple antibiotic resistance, at 2.3 Å resolution. *Nat Struct Biol* 8(8):710–714.
8. Saito K, Akama H, Yoshihara E, Nakae T (2003) Mutations affecting DNA-binding activity of the MexR repressor of *mexR-mexA-mexB-oprM* operon expression. *J Bacteriol* 185(20):6195–6198.
9. Saridakis V, Shahinas D, Xu X, Christendat D (2008) Structural insight on the mechanism of regulation of the MarR family of proteins: High-resolution crystal structure of a transcriptional repressor from *Methanobacterium thermoautotrophicum*. *J Mol Biol* 377(3):655–667.
10. Kumarevel T, Tanaka T, Umehara T, Yokoyama S (2009) ST1710–DNA complex crystal structure reveals the DNA binding mechanism of the MarR family of regulators. *Nucleic Acids Res* 37(14):4723–4735.
11. Chambers HF, Kartalija M, Sande M (1995) Ampicillin, sulbactam, and rifampin combination treatment of experimental methicillin-resistant *Staphylococcus aureus* endocarditis in rabbits. *J Infect Dis* 171(4):897–902.
12. Gedikoglu Y, Colak A, Benli K, Erbengi T (1993) Efficacy of ampicillin/sulbactam combination in experimental shunt infections caused by *Staphylococcus epidermidis*. A light and scanning electron microscope study. *J Neurosurg Sci* 37(1):19–23.
13. Roncoroni AJ, Schuster M, Bianchini HM, Damiano C (1983) Resistance of *Staphylococcus aureus* to methicillin. *Rev Argent Microbiol* 15(4):227–231.
14. Chambers HF (1997) Methicillin resistance in *staphylococci*: Molecular and biochemical basis and clinical implications. *Clin Microbiol Rev* 10(4):781–791.
15. Martins A, Cunha Mde L (2007) Methicillin resistance in *Staphylococcus aureus* and coagulase-negative *Staphylococci*: Epidemiological and molecular aspects. *Microbiol Immunol* 51(9):787–795.
16. Brewer NS (1977) Antimicrobial agents—Part II. The aminoglycosides: streptomycin, kanamycin, gentamicin, tobramycin, amikacin, neomycin. *Mayo Clin Proc* 52(11): 675–679.
17. Gray GS, Fitch WM (1983) Evolution of antibiotic resistance genes: the DNA sequence of a kanamycin resistance gene from *Staphylococcus aureus*. *Mol Biol Evol* 1(1):57–66.

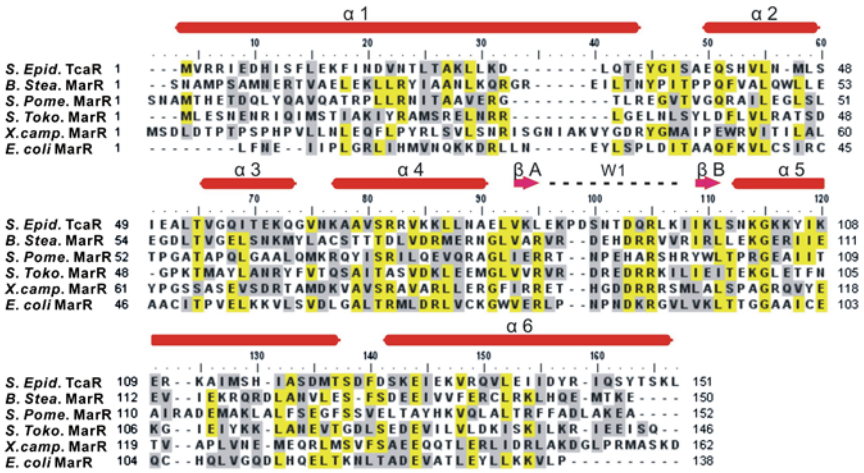

Fig. S1. Aligned sequences of TcaR from *S. epidermidis* with five marR family proteins. The numbers and secondary structure elements shown above the sequences are for the *S. epidermidis* TcaR and based on analysis of its crystal structure. The magenta arrows denote the locations of β-strands, and the red cylinders are for the α-helices. The conserved amino acids in the six sequences are shaded in yellow, and the similar residues are highlighted in gray.

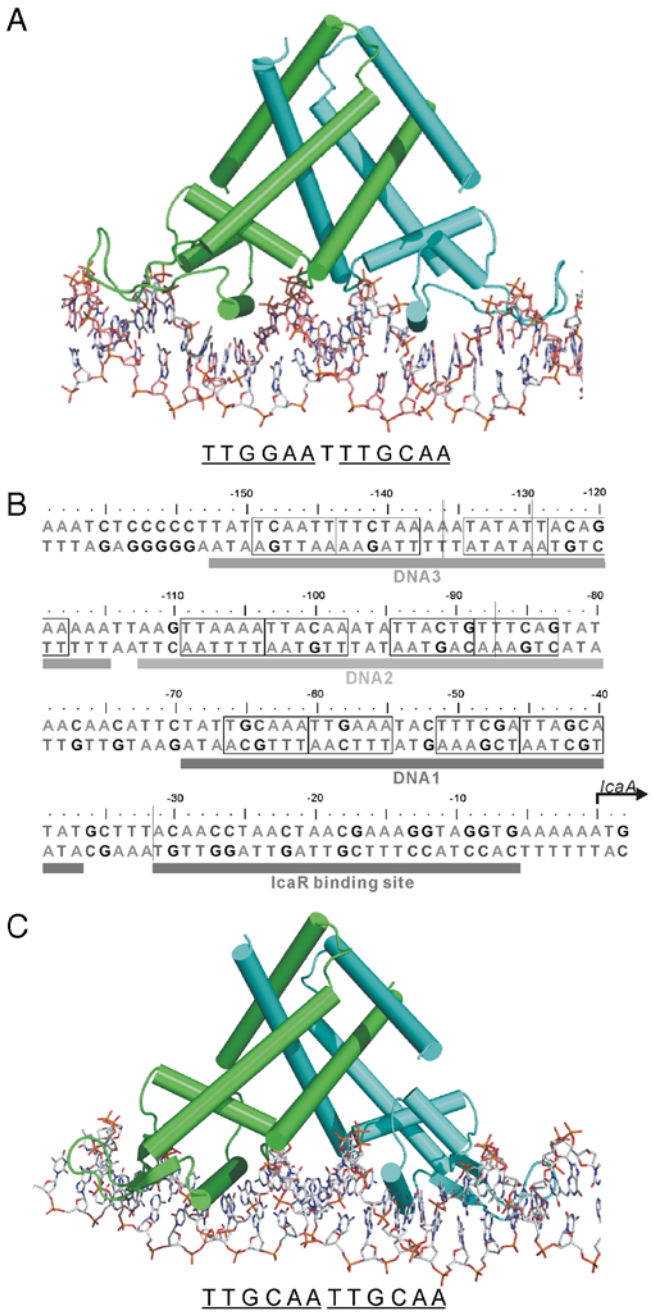

Fig. S2. The model of TcaR–DNA model. (*A*) The model of TcaR–DNA complex. The model was constructed based on the crystal structure of OhrR–ohrA complex (PDB 1Z9C) as a template. (*B*) DNA sequence of *ica* operon of *S. epidermidis*. The consensus sequences TTNNAA in another prediction mode are shown in black box. (*C*) The TcaR–DNA model was constructed based on the crystal structure of OhrR-ohrA complex (PDB 1Z9C) as a template, and the double strand DNA sequence was derived from (*B*).

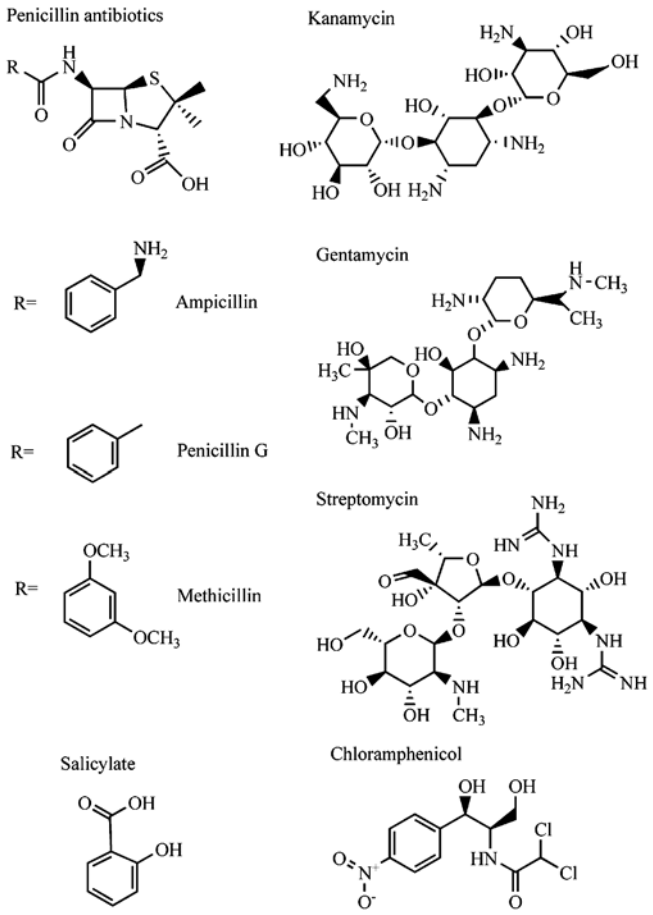

Fig. S3. List of the compounds used to test for the inhibition of TcaR. We use salicylate which is known to bind to and inactivate MarR in *E. coli*, beta-lactam antibiotics (penicillin G, ampicillin, and methicillin), aminoglycoside antibiotics (kanamycin, gentamicin, and streptomycin), and bacteriostatic antimicrobial (chloramphenicol) to test the inhibition effect of TcaR binding to DNA.

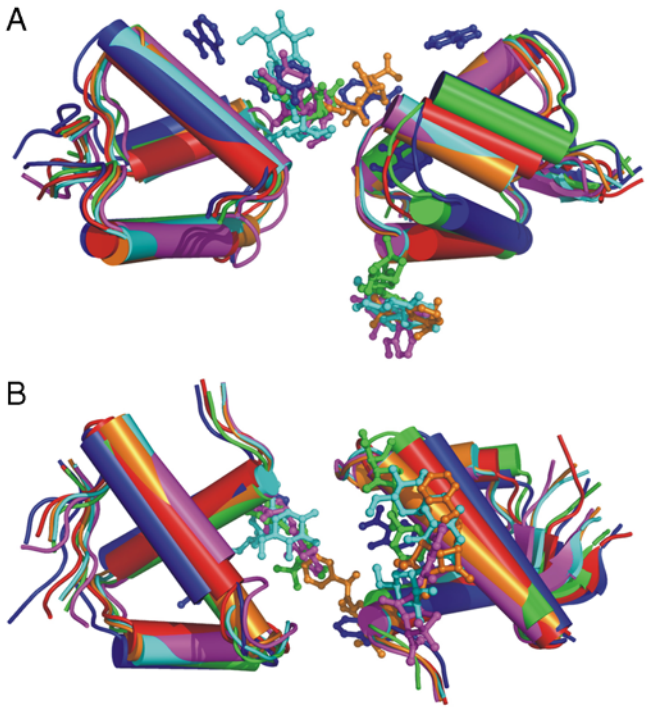

Fig. S4. (*A*) The enlargement of Fig. 3*E* showing the significant conformational change details at the wHTH domain. (*B*) The bottom view of (*A*).

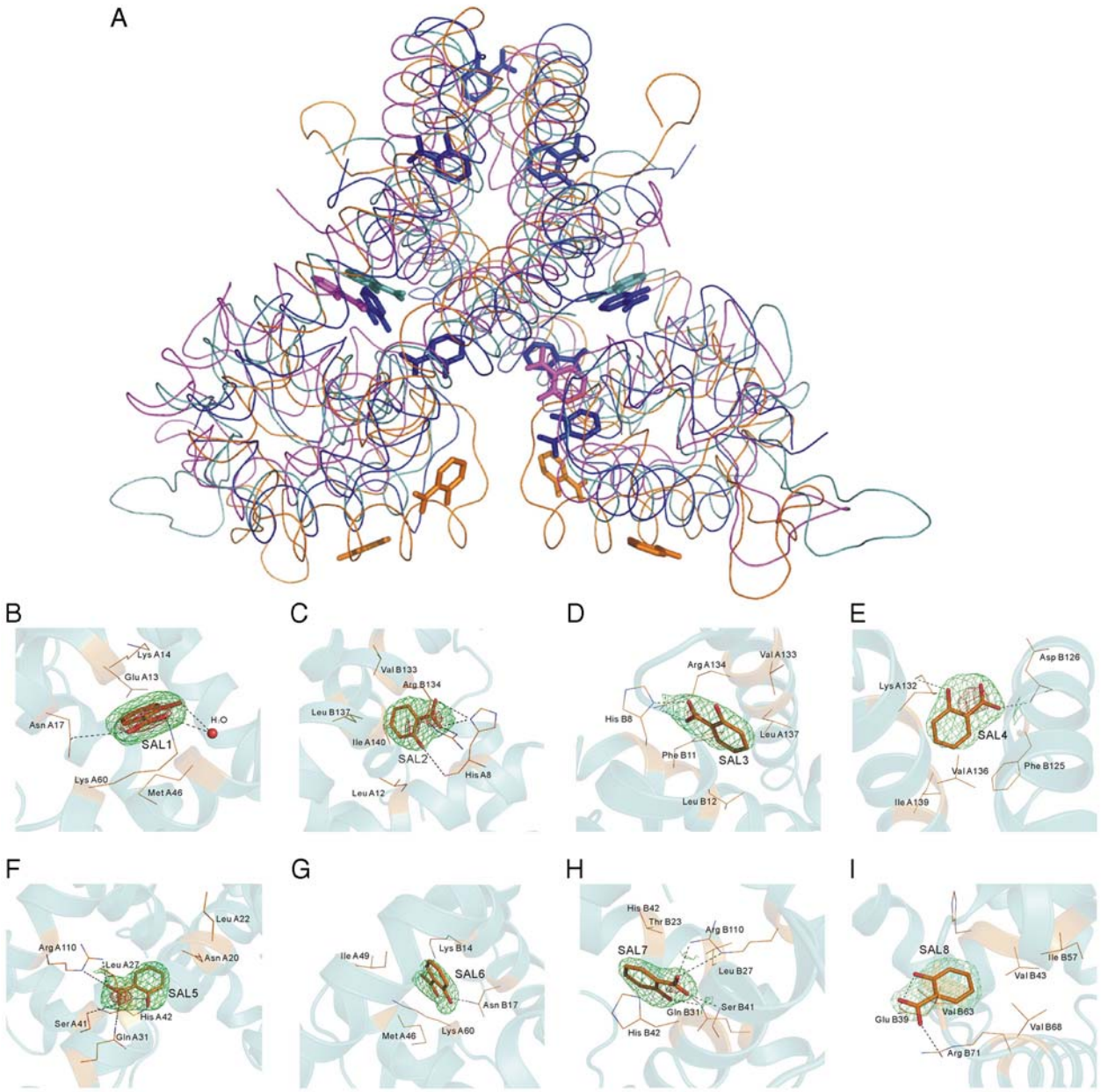

Fig. S5. (*A*) Comparison of the MarR–salicylate complex structures. The complexes of TcaR (blue), *E. coli* MarR (orange), *M. thermoautotrophicum* MarR (magenta), and *S. tokodaii* ST1710 (light teal) are superimposed. (*B–I*) A representation of some of the binding site residues relative to the bound salicylate in the binding pocket. As shown in (*B*), the first binding site of salicylate, SAL1 is formed by helix α1 of chain A and helices α′2 and α′3 of chain B. This site is composed of a high portion of charged residues including Glu A13, Lys A14, Asn A17, Met B46, Lys B60, and water. The SAL1 carboxylate forms hydrogen bond with the amino group of Lys B60 and the amide group of Asn A17. (*C*) The second binding site, SAL2 is formed by helix α1 of chain A and helix α′6 of chain B. This second binding site is formed by a high proportion of hydrophobic groups including His A8, Leu A12, Ile A140, Val B133, Arg B134, and Leu B137. The SAL2 carboxylate forms hydrogen bond with the imidazole group of His A8 and the guanidinium group of Arg B134. (*D*) The helix α6 of chain A and helix α′1 of chain B constitute the third binding site designated SAL3. This binding site consists of Val A133, Arg A134, Leu A137, His B8, Phe B11, and Leu B12. The SAL3 carboxylate forms hydrogen bond to the imidazole group of His B8 and the guanidinium group of Arg A134. (*E*) The fourth binding site, SAL4 is formed by helix α6 of chain A and the turn between helices α′5 and α′6 of chain B. The residues Lys A132, Val A136, Ile A139, Phe B125, and Asp B126 are the major interacting residues in this binding site. The SAL4 carboxylate hydrogen bonds the NH of backbone amide group of Asp B126 and the amino group of Lys A132. (*F*) In the fifth binding site, the residues that make up the binding site are formed from helices α1, α2 and α5 of chain A. The amino composition of this site includes Asn A20, Leu A22, Leu A27, Gln A31, Ser A41, His A42, and Arg A110. The SAL5 carboxylate hydrogen bonds the guanidinium group of Arg A110, the hydroxyl side chain of Ser A41, and the amide group of Gln A31. (*G*) The SAL6 binding site is composed of helices α2 and α3 of chain A and helix α′1 of chain B. This binding site consists of Met A46, Ile A49, Lys A60, Lys B14, and Asn B17. The SAL6 carboxylate hydrogen bonds the amide group of Asn B17 and the amide group of Lys B14. (*H*) The seventh binding site, SAL7 is formed by helices α′1, α′2, and α′5 of chain B. This binding site is composed of an even distribution of polar, charged, and hydrophobic residues including Thr B23, Leu B27, Gln B31, Ser B41, His B42, and Arg B110. The SAL 7 carboxylate group hydrogen bonds the amide group of Gln B31, the hydroxyl side chain of Ser B41, and the guanidinium group of Arg B110. (*I*) The eighth binding site, SAL 8 is exposed to the solvent and most contacts with salicylate are mediated by residues from the recognition helices α′2, α′3, α′4, and the turn between helices α′3 and α′4 of chain B. The amino composition of this site includes Glu B39, His B42, Val B43, Ile B57, Val B63, and Arg B71. The SAL 8 carboxylate group hydrogen bonds the guanidinium group of Arg B71 and the carboxylate group of Glu B39.

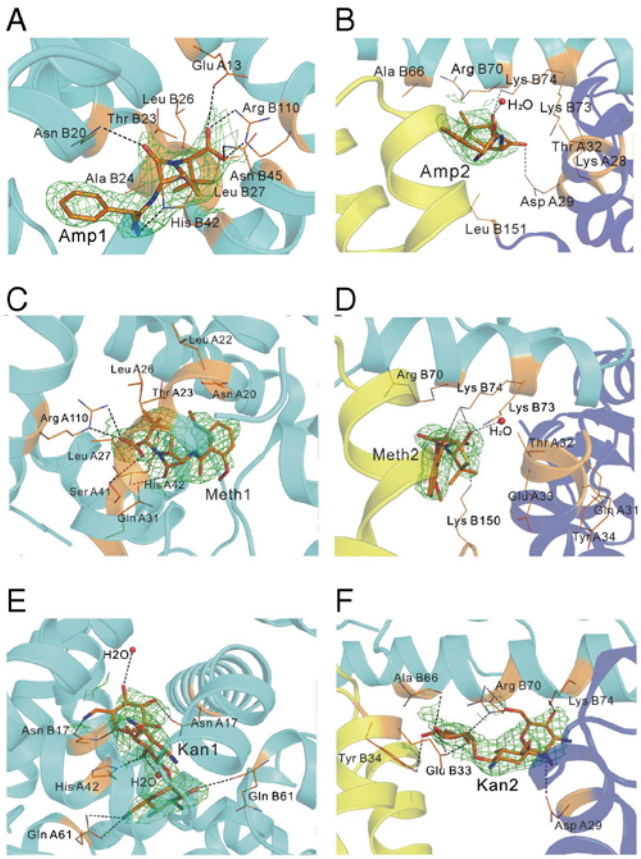

Fig. S6. (*A*) In the first Amp binding site (Amp1), Amp is surrounding by helix α1 of chain A and helices α′1, α′2, and α′5 of chain B. This site consists of Glu A13, Asn B20, Thr B23, Ala B24, Leu B26, Leu B27, His B42, Asn B45, and Arg B110. The carboxylic acid of the thiazolidine ring of Amp1 interacts with the side chains of residues Glu A13, Asn B45, and Arg B110, and the carbonyl group on the β-lactam ring hydrogen bonds to the amide group of Asn B20. Moreover, a hydrogen bond is also formed between the amide group of Amp1 and the imidazole group of His A42. (*B*) The second Amp binding site (Amp2) is formed by helix α′4 of chain B, helix α1 of chain A on the symmetry related molecule at the bottom left corner, and helices α1 and α6 of chain A on the symmetry related molecule at the bottom right corner like the orientation shown in Fig. 3*B*. The residues Ala B66, Arg B70, Lys B73, LysB74, and water in TcaR molecule, as well as Lys A28, Asp A29, Thr A32, and Leu B151 on the bottom right TcaR molecule forms interaction with Amp2. The carbonyl group on the β-lactam ring of Amp2 hydrogen bonds to the carboxyl group of Asp A29 and the carboxylic acid of thiazolidine ring formed hydrogen bonds with water and the amino group of Lys B72. (*C*) The first Meth binding site (Meth1) is comprised of helices α1, α2, and α5 of chain A which contains several Meth interacting residues: Asn A20, Leu A22, Thr A23, Leu A26, Leu A27, Gln A31, Ser A41, His A42, and Arg A110. The carboxylic acid of the thiazolidine ring of Meth1 interacts with the side chains of the residues Ser A41 and Arg A110, and the carbonyl group on the β-lactam ring hydrogen bonds to the NH of backbone amide group of His A42. (*D*) The second Meth molecule is located at the crystal contact formed by helix α′4 of chain B, helix α1 of chain A on the symmetry related molecule at the bottom left corner, and helices α1 and α6 of chain A on the bottom right molecule like the orientation shown in Fig. 3*B*. The residues in this binding site responsible for interacting with Meth2 include Arg B70, Lys B73, Lys B74, and water, as well as Gln A31, Thr A32, Glu A33, Tyr A34, and Leu B151 in the bottom right TcaR molecule. The carbonyl group of Meth2 hydrogen bonds to the amino group of Lys B74 and the carboxylic acid of the thiazolidine ring of Meth2 interacts with water and the side chains of residues Lys B74 and Lys B150. (*E*) The first binding site (Kan1) is formed by helices α1, α2, and α3 of chain A as well as helices α′1 and α′3 of chain B. The Kan molecule binds to this site through either ionic interactions or hydrogen bond interaction with Asn A17, His A42, Gln A61, Asn B17, Gln B61, and water. (*F*) The second Kan binding site (Kan2) is composed of helix α′4 of chain B, helix α1 of chain A on the bottom left molecule and helix α1 of chain A on the bottom right molecule like the orientation shown in Fig. 3*B*. The carbonyl group of the backbone of Ala B66 and polar residues including Arg B70, Lys B74, as well as Asp A29 on the bottom right TcaR molecule, and GluB33 and TyrB42 on the bottom left TcaR molecule are in the vicinity of Kan2 in a distance close enough to involve in ionic and hydrogen bond interaction.

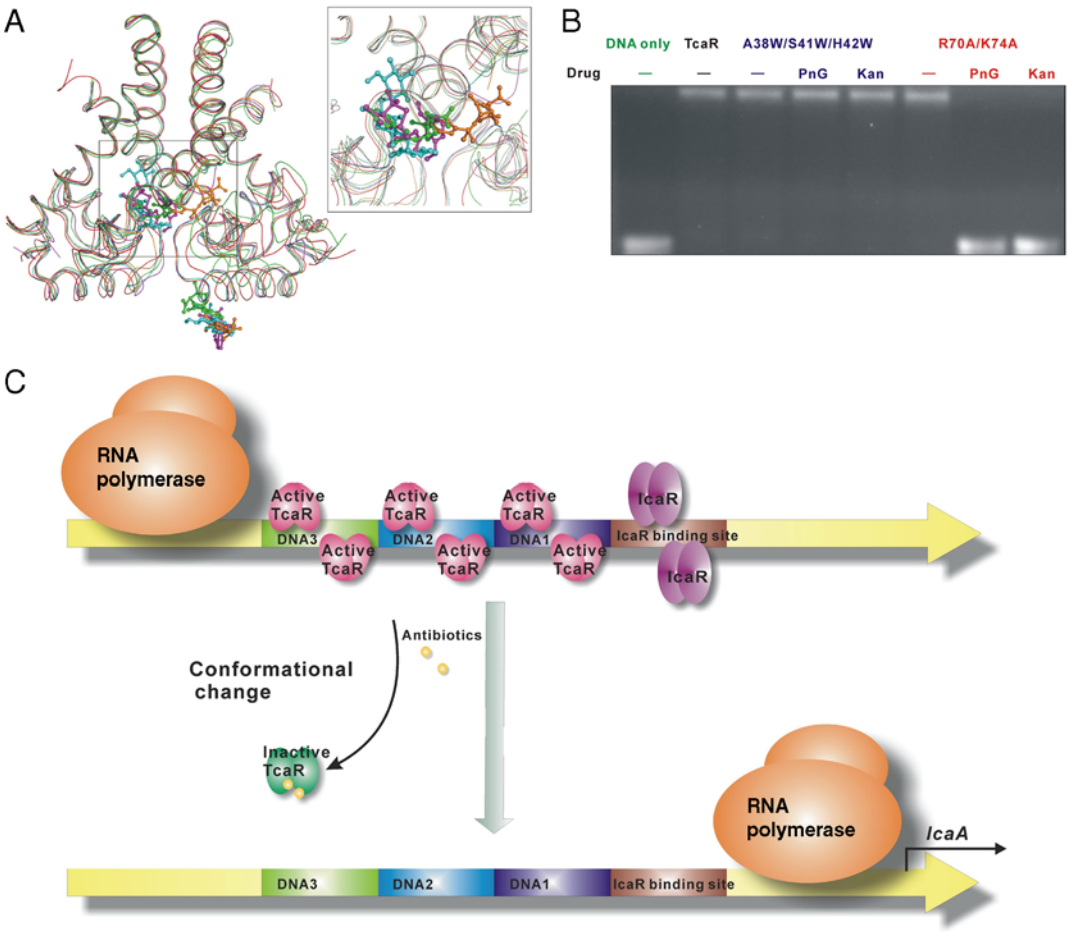

Fig. S7. (*A*) Superimposition of the apo (red) and the antibiotics-complexed structure of TcaR is shown as a worm tracing. The TcaR complexes of PnG (green), Amp (orange), Meth (magenta), and Kan (cyan) revealed a significant conformational change at the WH domain. The box in the upper right corner is the enlargement of the small box in center. (*B*) The effect of antibiotics on the TcaR mutant–DNA1 interaction. DNA1 probe duplex of 1 μM was preincubated with 4 μM of each TcaR mutant (dimer) at room temperature for 15 min before mixing with 4 μM antibiotics, followed by the same procedure done in the previous gel shift assays. (*C*) Illustration of the *IcaA* regulation mechanism. Under noninducing conditions, the active forms of TcaR and IcaR are capable of interaction with the *ica* operator and preventing transcription of *IcaA*. Upon entering of some antibiotics to the cell, significant conformational changes in the DNA binding domains of TcaR and IcaR will be exerted, inducing the inactivation and the departure of these transcriptional repressors from the *ica* promoter, thus increasing the expression of *IcaA*.

Table S1. Data collection and refinement statistics for the *S. epidermidis* TcaR crystals

Names	SeMet–TcaR	Native–TcaR
PDB number		3KP7
Data collection		
Wavelength (Å)	0.9793(peak)	1.0000
Space group	$P6_1$	$P6_1$
Resolution (Å)*	20-2.90 (3.00-2.90)	30-2.30 (2.38-2.30)
Unit cell cimensions		
$a = b$ (Å)	107.8	107.6
c (Å)	54.5	54.7
No. of reflections	8142(803)	16221(1590)
Completeness (%)	100.0(100.0)	99.9(100.0)
R_{merge} (%)	17.1(83.3)	7.0(78.3)
$I/\sigma(I)$	24.0(5.6)	34.1(2.5)
Phasing		
Resolution (Å)*	20-3.0	
Number of Se sites	6	
Z-score (SOLVE)	26.0	
Figure of meric (RESOLVE)	0.68	
Refinement		
No. of reflections		15393(1392)
R_{work} (95% data)		0.228(0.305)
R_{free} (5% data)		0.284(0.337)
Geometry deviations		
Bond lengths (Å)		0.018
Bond angles (°)		1.60
B-values (Å^2) number		
Protein atoms		53.5/2273
water atoms		58.9/118
Ramachandran plot (%)		
Most favored		95.1
Additionally allowed		4.9
Generously allowed		0.0

*Values in the parentheses are for the highest resolution shells.

Table S2. Data collection and refinement statistics for the *S. epidermidis* TcaR crystals

Names	TcaR–Sal	TcaR–Amp	TcaR–Kan	TcaR–Meth	TcaR–Png
PDB number	3KP6	3KP3	3KP5	3KP4	3KP2
Data collection					
Space group	$P6_1$	$P6_1$	$P6_1$	$P6_1$	$P6_1$
Resolution (Å)*	30-2.45 (2.54-2.45)	30-3.20 (3.31-3.20)	30-2.90 (3.00-2.90)	30-2.84 (2.94-2.84)	30-2.55 (2.64-2.55)
Unit cell dimensions					
$a = b$ (Å)	105.4	108.0	107.8	107.6	106.8
c (Å)	52.0	49.8	49.4	49.4	46.4
No. of reflections					
Observed	170071(12386)	18792(1808)	49797(1926)	36359(3553)	55516(5247)
Unique	12192(1126)	5615(548)	7318(642)	7703(756)	9969(990)
Completeness (%)	99.0(93.1)	99.8(100.0)	98.6(89.9)	97.9(98.3)	99.8(100.0)
R_{merge} (%)	7.3(55.1)	6.8(45.3)	6.5(40.1)	6.3(50.0)	6.2(40.0)
$I/\sigma(I)$	34.3(2.1)	19.2(2.9)	27.2(2.6)	22.7(3.0)	35.8(5.0)
Refinement					
No. of reflections	11500(934)	5348(499)	7048(604)	7384(663)	9688(894)
R_{work} (95% data)	23.4(31.1)	24.7(31.6)	23.3(30.6)	23.6(27.9)	23.3(28.5)
R_{free} (5% data)	27.1(31.2)	27.4(35.9)	27.6(51.5)	25.6(33.1)	27.1(35.0)
Geometry deviations					
Bond lengths (Å)	0.016	0.007	0.010	0.009	0.011
Bond angles (°)	1.4	1.3	1.5	1.5	1.5
No. of all protein atoms	2220	2193	2193	2222	2205
Mean B-values ($Å^2$)	60.6	54.7	56.7	59.6	59.8
No. of ligand atoms	85	48	66	52	51
Mean B-values ($Å^2$)	53.1	72.6	64.7	69.8	69.4
No. of water molecules	82	86	145	129	90
Mean B-values ($Å^2$)	66.7	36.4	56.1	53.6	72.6
Ramachandran plot (%)					
Most favored	92.3	88.3	90.7	93.4	93.0
Additionally allowed	7.3	11.3	8.2	6.2	6.6
Generously allowed	0.4	0.4	1.2	0.4	0.4

*Values in the parentheses are for the highest resolution shells.